Imaging the Transport Dynamics of Single Alphaherpesvirus Particles in Intact Peripheral Nervous System Explants from Infected Mice

Andrea E. Granstedt, Bingni W. Brunton,* Lynn W. Enquist

Department of Molecular Biology, Princeton University, Princeton, New Jersey, USA

* Present address: Bingni W. Brunton, Department of Biology and Department of Applied Mathematics, University of Washington, Seattle, Washington, USA.

ABSTRACT Alphaherpesvirus particles travel long distances in the axons of neurons using host microtubule molecular motors. The transport dynamics of individual virions in neurons have been assessed in cultured neurons, but imaging studies of single particles in tissue from infected mice have not been reported. We developed a protocol to image explanted, infected peripheral nervous system (PNS) ganglia and associated innervated tissue from mice infected with pseudorabies virus (PRV). This *ex vivo* preparation allowed us to visualize and track individual virions over time as they moved from the salivary gland into submandibular ganglion neurons of the PNS. We imaged and tracked hundreds of virions from multiple mice at different time points. We quantitated the transport velocity, particle stalling, duty cycle, and directionality at various times after infection. Using a PRV recombinant that expressed monomeric red fluorescent protein (mRFP)-VP26 (red capsid) and green fluorescent protein (GFP)-Us9 (green membrane protein), we corroborated that anterograde transport in axons occurs after capsids are enveloped. We addressed the question of whether replication occurs initially in the salivary gland at the site of inoculation or subsequently in the neurons of peripheral innervating ganglia. Our data indicate that significant amplification of infection occurs in the peripheral ganglia after transport from the site of infection and that these newly made particles are transported back to the salivary gland. It is likely that this reseeding of the infected gland contributes to massive invasion of the innervating PNS ganglia. We suggest that this "round-trip" infection process contributes to the characteristic peripheral neuropathy of PRV infection.

IMPORTANCE Much of our understanding of molecular mechanisms of alphaherpesvirus infection and spread in neurons comes from studying cultured primary neurons. These techniques enabled significant advances in our understanding of the viral and neuronal components needed for efficient replication and directional spread between cells. However, *in vitro* systems cannot recapitulate the environment of innervated tissue *in vivo* with associated defensive properties, such as innate immunity. Therefore, in this report, we describe a system to image the progression of infection by single virus particles in tissue harvested from infected animals. We explanted intact innervated tissue from infected mice and imaged fluorescent virus particles in infected axons of the specific ganglionic neurons. Our measurements of virion transport dynamics are consistent with published *in vitro* results. Importantly, this system enabled us to address a fundamental biological question about the amplification of a herpesvirus infection in a peripheral nervous system circuit.

Address correspondence to Lynn W. Enquist, lenquist@princeton.edu.

Alphaherpesvirus particles can transit over long distances in the nervous system in axons of synaptically connected neurons. Particles are transported bidirectionally within axons using specific molecular motors. In a prototypical infection of a natural host, an alphaherpesvirus will infect an epithelial layer, such as the epidermis/dermis of the skin or mucosa, sort particles into the innervating axon terminals, and travel by retrograde transport using dynein motors to establish a quiescent or latent infection in neurons of the innervating peripheral sensory ganglia. Upon reactivation, newly made particles usually spread back to the initial site of infection by anterograde transport in axons, forming a lesion in the epithelial cells. On rare occasions, the infection will spread to the central nervous system, usually resulting in serious or fatal brain inflammation. Herpes simplex virus (HSV) and

pseudorabies virus (PRV) are two alphaherpesviruses commonly studied to elucidate mechanisms of transport and spread of infectious particles. In humans, HSV-1 typically infects oral tissues and the eye, with subsequent quiescent infections of associated sensory and autonomic ganglia. In adult swine, PRV has a tropism similar to that of HSV; however, in nonnatural hosts (e.g., rodents, cattle, and dogs), PRV infection is invariably lethal and causes violent pruritus at the site of infection (the "mad itch"). Attenuated strains of PRV that lack the ability to cause this peripheral neuropathy are neuroinvasive and spread efficiently to the central nervous system (CNS) from the periphery (1). Such strains have been exploited as tracers of neuronal circuitry and are of considerable interest to the neuroscience community (2).

Cultured neurons have been invaluable for defining molecular

and cellular mechanisms of infection, particularly in measuring the dynamics of viral particle transport and spread in axons. Similar studies in living infected animals, however, have been technically challenging. Investigators historically approximated the rate of axonal transport based on the time when infection was initiated at axon terminals or symptoms were first indicated in the periphery to the time when viral replication in neuron cell bodies was apparent. These studies have estimated rates ranging from 42 mm/day in young mice (3) to 240 mm/day in calves (4). More recently, an important study calculated the velocity of varicella-zoster virus particle movement in humans to be approximately 1.5 μm/s based on a clinical report of a zoster occurrence involving the sciatic nerve of a patient (5). Other studies of HSV-1 particle motion used preparations of the squid giant axon to calculate the retrograde transport velocity to be 2.2 μm/s (6). In dissociated chick dorsal root ganglia, Smith et al. measured the anterograde velocity of PRV to be 1.97 μm/s (7).

For some of the *in vitro* studies mentioned above, primary neurons are harvested from embryos and are grown in a simplified and artificial environment, absent of natural synaptic partners. These relatively pure cultures of neurons lack supporting cells as well as the structure and associated nonneuronal tissues that characterize the natural site of infection. In addition, in these *in vitro* systems, virions are usually added directly to the cell bodies and axons, a process which is different from a natural infection in which virions invade peripheral tissue and enter the nervous system through innervations of the target tissue. In this report, we expanded our previous work to develop a system to image and determine the transport dynamics of individual PRV virions in intact innervated tissue after infection of the rodent salivary gland (23). With this preparation, we were able to track unambiguously the transport dynamics of fluorescently tagged, individual PRV virions over time.

This *ex vivo* preparation not only enabled us to validate the previous *in vitro* findings but also provided an opportunity to explore the biology of invasion of the peripheral nervous system. One outstanding question we addressed is the relative significance of replication at the site of infection and its contribution to the invasion of the innervating peripheral ganglion neurons. As these neurons ultimately will harbor the latent or acute infection, they are the critical interface for subsequent spread to the central nervous system. While PRV is known to be taken up directly at axon terminals (9), it also can replicate extensively in the peripheral epithelia at the site of inoculation (10). For HSV, it has been proposed that during the acute phase of infection in the skin, virions make a "round trip" from the skin to the innervating ganglion and back before the latent infection is established. In this model, the secondary invasion of the inoculation site may produce lesions and more virions for further seeding of the ganglion (11). Accordingly, viral amplification might first occur in the peripheral ganglia after a few virions invade the neurons. Some have argued that upon reactivation of a latent infection, newly replicated virions will make round trips from the ganglia to the skin and back again, thereby infecting and populating new neurons in each recurrence (12). We were able to observe such round-trip movement during PRV infection using our *ex vivo* preparation. We propose a model for how the infection is amplified in the circuit, which may explain both the peripheral neuropathies characteristic of herpesvirus infections and disease progression *in vivo*.

RESULTS

Imaging viral particles in acutely explanted tissue. We infected the salivary glands of adult male mice with PRV 180 as described in Materials and Methods. PRV 180 is a virulent PRV recombinant isogenic strain with PRV Becker in which the VP26 minor capsid protein was fluorescently tagged with monomeric red fluorescent protein (mRFP) (13). Infected tissue explants from these infected mice were analyzed at 12, 24, or 48 h after infection. At the desired time point, the mice were euthanized and an intact section of infected tissue that included the salivary glands, ducts, and submandibular ganglia (SMG) was removed. The infected tissue with exposed SMG was oriented and pinned down into a Sylgard-coated, glass-bottom dish for epifluorescence imaging (Fig. 1A).

The orientation of the tissue was kept constant across all imaging experiments so that the direction of particle movement to and from the gland and SMG was able to be determined unambiguously. The imaging window was maintained at a fixed height and width with the axon bundles aligned horizontally. The SMG clusters in each animal differ in number and orientation along the salivary duct such that comparing any one SMG between animals is difficult. Accordingly, we positioned the imaging window as closely as possible to the same area between accessible SMGs and the salivary glands (Fig. 1A, magnified panel).

As described in Materials and Methods, 100 particles were tracked for each explanted tissue using the ImageJ plug-in MTrackJ (14). The data were pooled across the tissue from three animals collected for each time point. All particles transiting to the left (toward the salivary gland) were scored as anterograde-moving particles, and those moving to the right (toward the SMG cell bodies) were scored as retrograde-moving particles. Particles that did not move for the duration of the movie were labeled as stationary. Figure 1B is a cropped area taken from a sample movie and displays panels from every 10 frames. In this particular view, particle 1 (orange) is moving in the anterograde direction, particle 2 (yellow) is stalled, and particle 3 (green) is moving in the retrograde direction (Fig. 1B). The data were further analyzed using custom code written in Matlab to calculate velocity, processivity, and other features.

The majority of virions travel back to the glands by 12 h after infection. To examine the net transport and directionality of fluorescently tagged particles (Fig. 2A), each tracked particle was categorized as traveling anterograde (back to the gland), traveling retrograde (toward the neuronal cell bodies), or stationary. Some particles paused or changed their directions of travel temporarily during the imaging sessions, so we considered only the net direction of travel between the first and the last frame where the particle was tracked. A particle was considered stationary if it remained stalled throughout the movie (see Movies S1 and S2 in the supplemental material).

Several interesting features emerged (Fig. 2A): first, more particles were moving in the anterograde direction at 12 h than at 24 or 48 h. Conversely, fewer particles were moving in the retrograde direction. At 12 h, 84% of particles had an anterograde trajectory while 16% had a retrograde trajectory. At 24 and 48 h, 67% and 64% of particles were traveling in the anterograde direction, respectively, and 31% and 32% of particles were traveling in the retrograde direction, respectively. These observed differences at 12 h were statistically significant (Fig. 2A). Also at 12 h, movement was highly processive, with most particles traveling without paus-
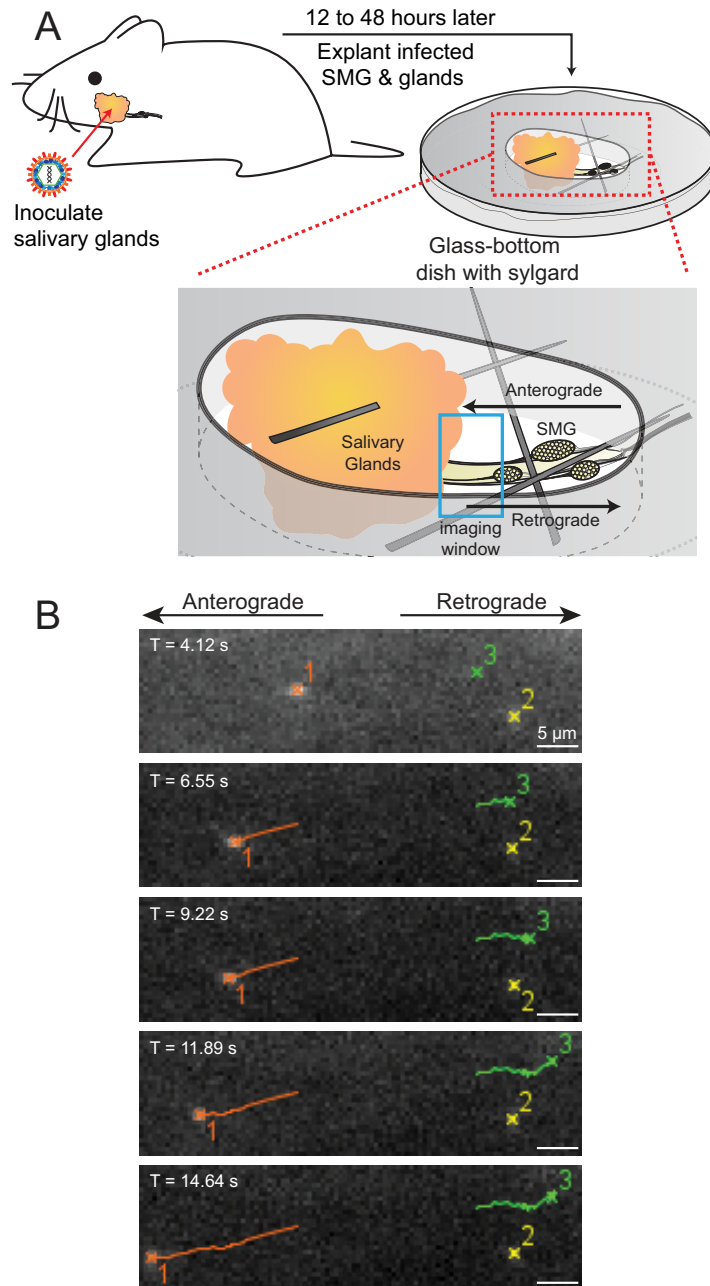
FIG 1 *Ex vivo* imaging setup and tracking of viral particles. (A) Diagram to illustrate how the infection is initiated in the mouse by inoculating the salivary glands, and then at various times after infection, the infected tissue is explanted and placed in a glass-bottom dish. The dish was prepared by coating it with Sylgard and cutting a hole over the glass coverslip in order to visualize the progression of infection through the tissue on a standard inverted epifluorescence scope. The sample was pinned down firmly and flattened using fine needles that were held in place by piercing the Sylgard. The magnified panel shows the approximate imaging window and the directions, defined as anterograde and retrograde. (B) Panels represent a cropped area taken from a sample movie every 10 frames. The exact time of acquisition within the movie is indicated. In this view, three particles are tracked: particle 1 (orange) is moving anterograde, particle 2 (yellow) is stalled, and particle 3 (green) is moving retrograde. Scale bars are consistent in all frames.

ing or stalling through the entire imaging window. In contrast, at 24 and 48 h, processivity was more variable (data not shown). In addition, stationary particles were more frequent at 24 and 48 h (2% and 4% of total particles, respectively), and this difference was significant between 12 and 48 h (Fig. 2A). We will discuss the source of the substantial number of particles moving back to the salivary gland (anterograde direction) below.

Particles at 12 h after infection spend more time in transit. Next we looked at the fraction of time each particle spent moving versus pausing (Fig. 2B). The trajectory of each particle was subdivided into anterograde, retrograde, and stalled parts. Stalls were empirically identified as frames in which the mean displacement over the last two time points was less than 0.8 pixels (0.21 μm). Movements in the anterograde and retrograde directions are ex-
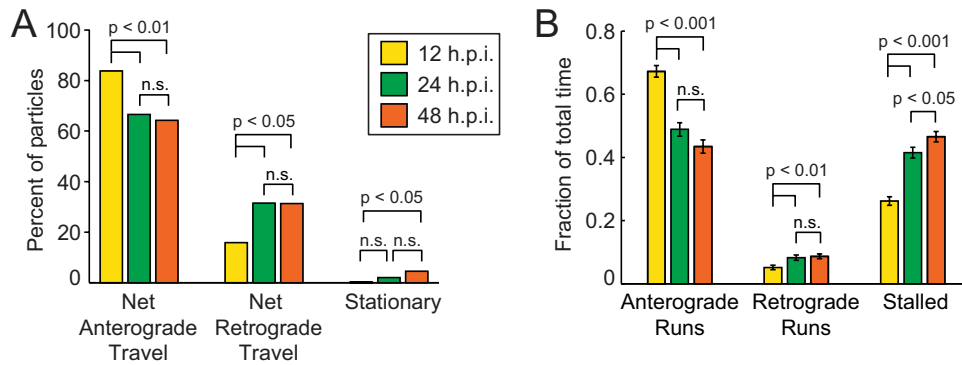
FIG 2 Quantitative analysis of particle directionality and duty cycle. (A) Analysis of the net direction of transport at 12, 24, and 48 h postinfection (h.p.i.). Colors corresponding to each time point are indicated in the inset box. Net anterograde and retrograde directions were analyzed separately, and the percentage of particles transiting in each direction is displayed. Particles that did not move for the duration of the movie were labeled as stationary. (B) Analysis of the fraction of time that the particles spent transiting versus stalling at 12, 24, and 48 h postinfection. Colors corresponding to each time point are indicated in the inset box in panel A. Statistical significance with the P value is indicated; n.s., not significant.

pressed as a fraction of the total time each particle was tracked. At 12 h, particles moved in the anterograde direction 0.67 ± 0.018 (mean $\pm$ standard error of the mean [SEM]) of the time; at 24 and 48 h, anterograde movement was observed 0.49 ± 0.021 and 0.43 ± 0.021 of the time, respectively. Retrograde movement was observed at 12, 24, and 48 h 0.051 ± 0.0070, 0.083 ± 0.0084, and 0.087 ± 0.0077 of the time, respectively. Particles were stalled at 12, 24, and 48 h for 0.26 ± 0.014, 0.41 ± 0.017, and 0.46 ± 0.016 of total tracked time, respectively. These three measurements at 12 h were statistically different from measurements at 24 and at 48 h. In other words, particles were in motion (i.e., not stalled) for more of the time at 12 h and were more likely to move in the anterograde direction than they were at later time points.

The velocity of moving particles is similar across all time points. To measure the velocity of virions during transit, we split up the trajectories of tracked particles into anterograde and retrograde runs separated by stalls and then we calculated the velocity in micrometers traveled per second in each direction (Fig. 3). Not all tracked particles had both anterograde and retrograde runs, so the total number of particles in transit in each direction varied. In fact, there were far fewer retrograde runs, especially at 12 h after infection. We saw no appreciable difference in anterograde or retrograde velocity at any time after infection. The mean anterograde speeds were 1.94 ± 0.032 (mean $\pm$ SEM across particles), 1.85 ± 0.041, and 1.90 ± 0.041 μm per second at 12, 24, and 48 h, respectively. The mean retrograde speeds were 0.82 ± 0.028, 1.06 ± 0.028, and 1.04 ± 0.025 μm per second at 12, 24, and 48 h, respectively. There was no statistically significant difference in the velocity measurements across all time points, and therefore, not surprisingly, the virions likely use the same molecular motors regardless of the time after infection.

Particles stall for longer durations at later time points after infection. All particles were moving at 12 h, with only intermittent stalls or pauses, but as the time after infection increased, we observed more particles that did not move for the duration of the movie, which we considered stationary particles (Fig. 2A). However, the number of intermittent stalls per second was consistent across time points, and any particle was just as likely to stall as any other. The stall frequencies for 12, 24, and 48 h were 0.014 ± 0.00048, 0.014 ± 0.00043, and 0.014 ± 0.00043 (mean $\pm$ SEM across particles) per second, respectively (Table 1). However, the

duration of intermittent stalls, in which stalled particles did regain motion in either direction, varied significantly. The mean durations of stalls at 12, 24, and 48 h after infection were 1.40 s (median = 0.5 s), 2.13 s (median = 0.75 s), and 2.03 s (median = 1.0 s), respectively (Table 1). Thus, even though the probability of stalling intermittently was the same at all times after infection, parti-
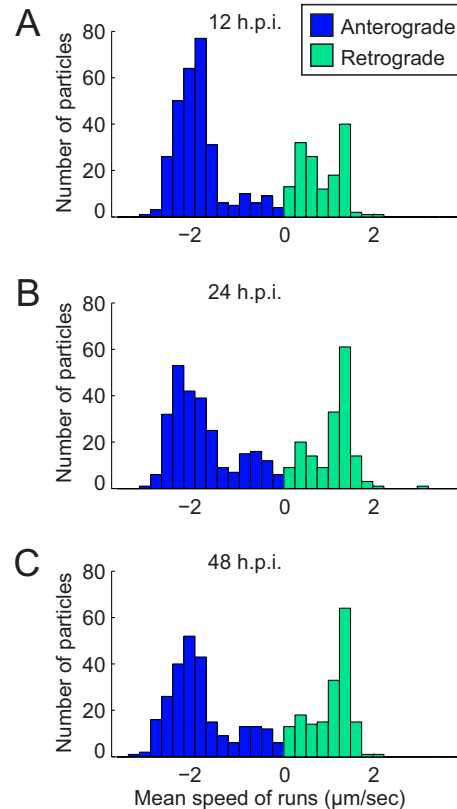

FIG 3 Quantitative analysis of particle velocity. Histogram of particle velocity in anterograde and retrograde directions at 12 (A), 24 (B), and 48 (C) h postinfection (h.p.i.). The numbers of micrometers traveled per second were calculated in each direction during the frames that the particles were in motion. The colors corresponding to the different directions are indicated in the inset box.

TABLE 1 Frequency and duration of stalls and runs at different times post infection

Stall or run characteristic	Value at each time post infection		
	12 h	24 h	48 h
Stall frequency[a]	0.014 ± 0.00048	0.014 ± 0.00043	0.014 ± 0.00043
Duration of stalls[b]	1.40 ± 2.47	2.13 ± 4.60	2.03 ± 3.55
Duration of anterograde runs[b]	2.81 ± 3.80	2.39 ± 3.26	2.37 ± 3.05
Duration of retrograde runs[b]	0.76 ± 0.81	0.79 ± 0.72	0.82 ± 0.82

[a] In units of 1/s; values are means ± SEM.
[b] In seconds; values are means ± standard deviations.

cles spent more time stalled at 24 and 48 h than at 12 h after infection. Increased stalling as infection proceeds might reflect increased metabolic requirements or intrinsic limitations of the transport machinery.

We also calculated the duration of runs in both the anterograde and retrograde directions. At 12 h after infection, anterograde runs were longer; the means at 12, 24, and 48 h were 2.81 ± 3.80 s (mean ± standard deviation), 2.39 ± 3.26 s, and 2.37 ± 3.05 s, respectively (Table 1). The standard deviation reflected the short-run distance. In contrast, retrograde runs did not vary after infection, though the run durations were shorter in the retrograde direction than in the anterograde direction: the mean values were 0.76 ± 0.81 s (mean ± standard deviation), 0.79 ± 0.72 s, and 0.82 ± 0.82 s for 12, 24, and 48 h, respectively (Table 1). The slower mean retrograde velocity may result from the reduced processivity.

Infection with a PRV strain that cannot sort virus particles into axons. As noted above, by 12 h after infection, a substantial number of particles were moving in the anterograde direction back to the site of infection in the salivary gland. The following experiments help explain this perhaps-unexpected result. PRV Bartha is commonly used as a retrograde tracer for neuronal circuit mapping (2). Infection with PRV Bartha derivatives moves only from postsynaptic to presynaptic neurons in a circuit because newly replicated particles are not sorted into axons and are not available for anterograde transport to presynaptic sites (1). Importantly, PRV Bartha has been used to map the salivary circuitry after injection into salivary glands (8), proving that it replicates and spreads well in the salivary gland circuitry, but only in the retrograde direction. We infected the salivary glands of mice with

PRV 765, a recombinant of PRV Bartha for which the VP26 minor capsid protein was fluorescently tagged with monomeric red fluorescent protein (mRFP) (15). Infected salivary gland and SMG tissues were explanted and imaged at 24 or 48 h after infection (Fig. 1A). In contrast to the virulent PRV 180 infection, we rarely saw any directed particle movement in any direction over long distances in axons of tissue infected with PRV 765 at 24 or 48 h postinfection. Occasionally a rare particle would make a short run, but more often, the particle motion resembled random undirected Brownian motion (see Movie S3 in the supplemental material).

Despite our efforts, we have been unable to image the primary retrograde infecting particles early after infection from the gland. We believe that infection involves a small number of particles distributed over many axons in a large area, which makes imaging them challenging. We therefore conclude that the infected SMG neurons that project to the gland are the source of the abundant PRV 180 particles 12 h after infection. As we will discuss below, the retrograde transport events observed during the virulent infection most likely represent second-round transport to the ganglia after round-trip infection.

Infection with a PRV recombinant that expresses both an mRFP-tagged capsid protein and a GFP-tagged envelope protein. We infected mice with PRV 341, a virulent PRV Becker recombinant in which the minor capsid protein VP26 was fused to mRFP and the envelope protein Us9 was fused to green fluorescent protein (GFP) (16). Qualitatively, we observed that all the anterograde-moving red capsid puncta were colabeled with Us9-GFP (Fig. 4; see also Movie S4 in the supplemental material). We also detected green puncta that were not colocalized with red
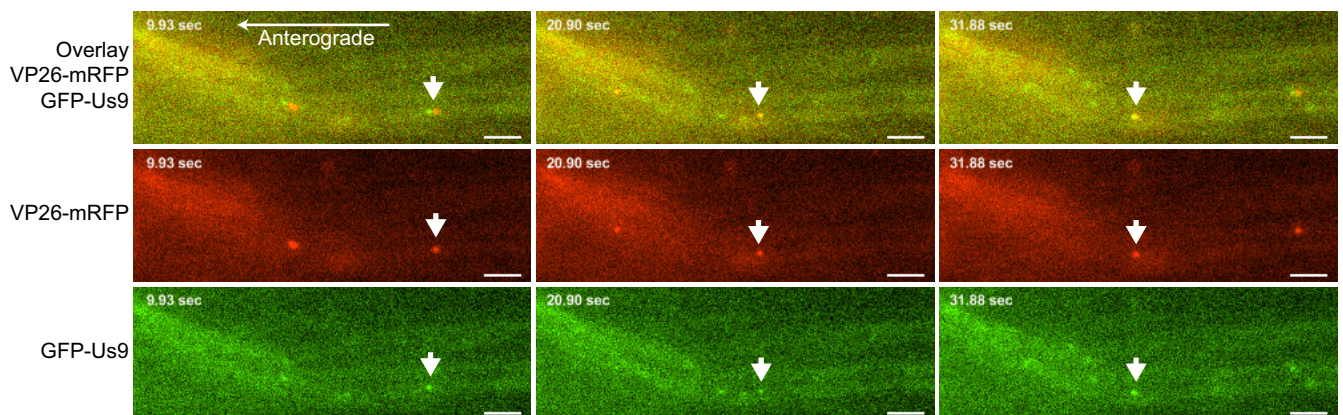

FIG 4 Anterograde-moving particles with a red capsid tag are also GFP positive. Representative frames from Movie S4 in the supplemental material with the capsid tag VP26-mRFP, the envelope tag GFP-Us9, and an overlay of the two fluorescence channels, as labeled. Arrows point to a dual-fluorescence viral particle traveling anterograde. Direction is indicated. Scale bars are consistent in all frames and are equal to 5 μm.

puncta, but we did not detect red-only puncta. These data support our contention that the viral particles moving in the anterograde direction back to the gland arose from replication events in the ganglia and that sorting into the axonal compartments occurred after envelopment.

DISCUSSION

The *ex vivo* preparation described in this report was developed to approximate an *in vivo* infection for the measurement of transport dynamics of viral particles. The salivary circuit has proved to be useful because of its accessibility for infection and harvesting of tissues. It has also been used extensively for repeated imaging experiments to locate and study the same nerve cells in a living mouse at different time points (17). The preparation resembles a more natural scenario since infection initiates and proceeds in the animal prior to analysis. Importantly, the dissection retains the gland and its innervating ganglia and connected axons intact. We present qualitative and quantitative data of PRV particle transport dynamics in infected, explanted salivary gland and SMG tissues. Since the tissue orientation was held constant and the imaging window was set to be between the neuron cell bodies of the SMG and the intact target salivary glands, we were able to directly infer the direction of transport of viral particles as being toward the gland (anterograde direction) or toward the SMG (retrograde direction).

The first important findings are that the details of velocity, duty time, and stalling of infecting virus particles are not dramatically different from values determined in cultured neurons from chick neurons (7). Our observations of transport and stalling behavior are also consistent with *in vitro* results demonstrating that PRV uses KIF1A, a microtubule-dependent kinesin-3 motor, for axonal sorting and anterograde transport (18). Using a PRV recombinant that expresses a fluorescent capsid and envelope protein, we showed that the anterograde-moving capsid puncta were newly replicated since they were colabeled with the viral membrane protein. These findings are also consistent with the model that suggests that capsids are sorted into axons after envelopment (16, 19). Since the infection occurred in a living animal prior to analysis, we can conclude that tissue architecture and local defenses in the salivary gland or associated tissues have little or no discernible effect on dynamics of virus particle transport. Transport is almost entirely a cell-autonomous process.

The second important finding is that this preparation provides interesting observations about invasion of the peripheral nervous system that could not have been discerned from standard *in vitro* experiments. Our initial expectation was that particles would invade the SMG, replicate, and then continue on to spread into the CNS. However, we were surprised to see abundant viral particles at 12 h after infection moving back to the salivary gland, implying that they had replicated in the neuronal cell bodies and had now reversed their direction. This process would reinfect the salivary gland, and the progeny from this second amplification would continue to infect more neurons in the many SMG clusters that project to the salivary gland. Though we are unable to image the salivary glands directly for technical reasons, we predict that viral expansion in the gland would follow these reseeding events. Consistent with this prediction, we see increasing numbers of SMG neurons infected at later times after infection (data not shown) (Fig. 5A to C).

Evidence for this round-trip reseeding model came from infections with a replicating PRV mutant that cannot sort virions into the axon and is incapable of anterograde spread of infection (the PRV Bartha derivative PRV 765). No anterograde-moving particles and only rare retrograde-moving particles are seen at any time after infection with PRV 765. This result is informative since PRV 765 does infect, replicate, and spread in these animals, ultimately killing them. Importantly, PRV Bartha (the parent of PRV 765) had been used extensively to map the salivary gland circuitry in rodents that projects to the salivary gland (8). Because PRV 765 and PRV Bartha cannot move particles into axons after replication in neuronal cell bodies, they should not perform the round trip from gland to SMG to gland and subsequent amplification in the gland would not occur (Fig. 5D).

The biology of PRV infection is well known (20, 21). Virulent PRV (e.g., PRV Becker) affects the peripheral nervous system of most nonporcine mammals before death, producing a pronounced peripheral neuropathy (violent pruritus or the "mad itch") with minimal transport to the brain (10). Our data suggest that virulent PRV primarily travels back and forth from the salivary glands and the peripheral nervous system neurons that innervate the gland. The result of this round-trip phenomenon is massive infection of peripheral neurons after a primary infection, which may be responsible for the noteworthy peripheral neuropathy induced by virulent PRV but not attenuated strains like PRV Bartha.

MATERIALS AND METHODS

Viruses and cells. The PRV Becker recombinants PRV 180 and PRV 341 were previously described (13, 16). The PRV Bartha recombinant PRV 765 was also previously described (15). All viruses were propagated, and titers were determined in PK15 (porcine kidney epithelial) cells. Viral stocks were concentrated before inoculation into animals.

Infection of the salivary circuit. All animal procedures were performed in accordance with the guidelines of the National Institutes of Health and were approved by local authorities (Princeton University Institutional Animal Care and Use Committee). The model for mouse SMG infection was previously described in detail (22, 23). Briefly, mice of ages 3 to 5 months were anesthetized with a mixture of ketamine (100 mg/kg of body weight) and xylazine (10 mg/kg) by intraperitoneal administration. A midline incision was made along the neck, exposing the salivary glands. Using a Hamilton syringe, concentrated PRV inoculum (10^9 PFU/ml) was injected into both submandibular glands (6 μl/side). The incision was sutured, and the mice were given a dose of buprenorphine (100-μg/kg concentration) against postsurgical pain. The mice were allowed to recover for various times postinoculation.

***Ex vivo* preparation.** At the desired time after infection, the animal was deeply anesthetized, and the material encompassing the glands, ducts, and SMG was removed intact; to explant this sample, layers of connective tissues were pulled away with fine forceps to separate the glands, ducts, and SMG from surrounding structures, and a cut was made near the digastric muscle. The animal was immediately sacrificed by thoracotomy, and the tissue was further dissected to expose the SMG. A MatTek glass-bottom dish (MatTek Corporation, Ashland, MA) was prepared by coating with Sylgard and cutting a hole over the glass coverslip in order to visualize the infection on a standard inverted epifluorescence microscope. The sample was pinned down firmly using fine needles that were able to be held in place by piercing the Sylgard. The needles also served to flatten the tissue to increase the optical range of the objective through the thick sample. The area was filled with warmed Neurobasal medium (Gibco) supplemented with 1% (vol/vol) penicillin/streptomycin-glutamine (Invitrogen) and B27 supplement (Invitrogen). Depending on the type of analysis performed, the objective was heated and a stage top incubator system was put in place to maintain a stable temperature and humid
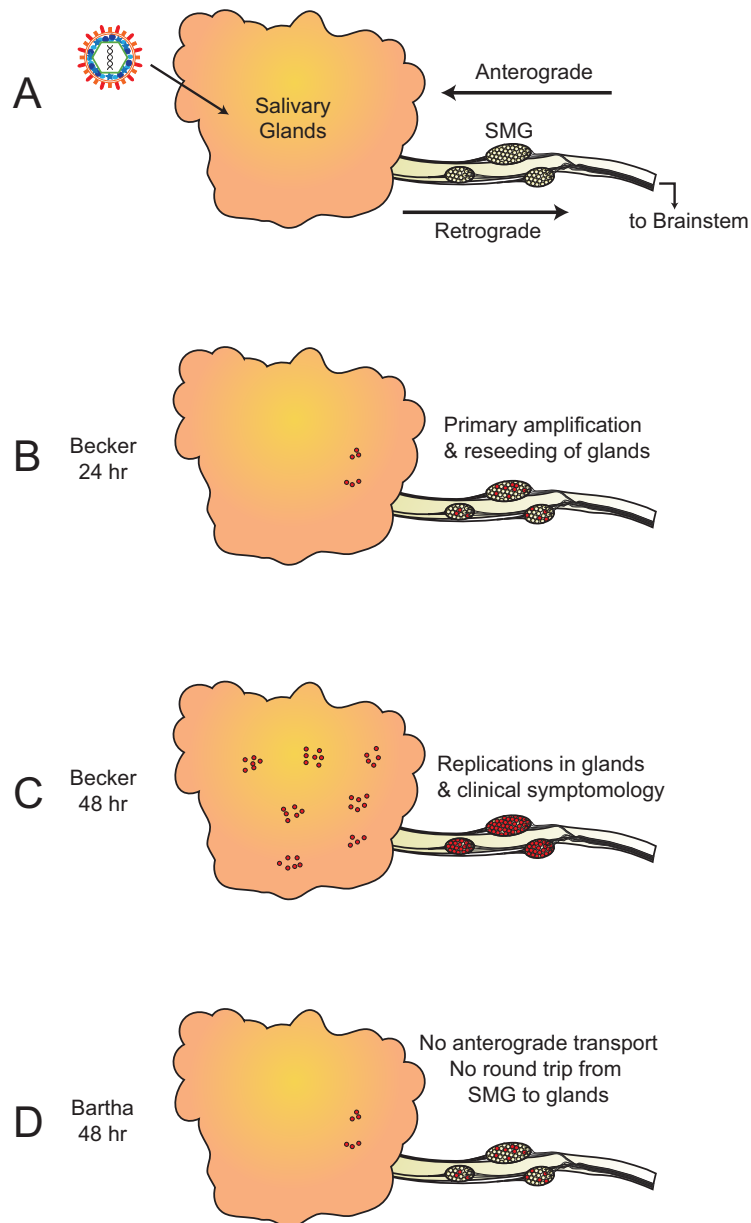
FIG 5 Model of virulent PRV (pseudorabies virus) amplification in the salivary circuit. (A) Infection is initiated in salivary glands. The submandibular ganglia (SMG) innervate the glands. Directionality of viral transport is indicated. (B) Based on our data, virions from the original inoculum are efficiently sorted into axon terminals and transported to the SMG neurons, where replication occurs and the infection is amplified. The newly made infectious particles are then transported in the anterograde direction back to the glands to reseed the infection in the glandular cells. (C) By 48 h after infection, all neurons in the SMG are infected and the animals display characteristic symptoms of mad itch. (D) The attenuated Bartha strain is deficient for anterograde spread, and therefore, particles that are replicated in the neurons will not be transported back to the glands but will continue to spread to the brainstem.

environment. In that case, after the dissection and preparation of the sample for imaging, the dish was left to equilibrate for 15 min on the stage before the imaging was started, and therefore, the time between when the tissue was explanted to when imaging began was approximately 30 to 40 min.

Image acquisition and data analysis. Movies were acquired on a Nikon Ti-Eclipse epifluorescence inverted microscope with a 60× Plan Fluor Ph3 objective (Nikon) at 37°C in a 5% (vol/vol) CO_2-enriched atmosphere using a stage top incubator system (Live Cell Instrument/Quorum Scientific). Images were acquired with an iXon 895 back-thinned electron multiplying charge-coupled device (EM-CCD) camera (Andor, Belfast, Northern Ireland). We used a broad-spectrum high-pressure

mercury fluorescence source and an mRFP filter set (Chroma; 89006 filter series). This system is also equipped with separate fast-switching excitation and emission filter wheels to enable rapid serial acquisition of multiple fluorescence channels. The imaging window was maintained at a fixed height of 100 pixels and width of 300 pixels. The fluorescence exposure was set to 200 ms, with the EM Gain filter set to 300. The acquisition rate was approximately 4 frames per second, on average. For the dual fluorescent movies, the exposure was set to 300 ms and the acquisition rate was approximately 1 frame per second. The movies ranged from 2 to 5 min in length. The raw data were visualized in ImageJ (W. S. Rasband, ImageJ, National Institutes of Health, Bethesda, MD; http://rsb.info.nih.gov/ij/), and particles were manually tracked in infected axons using the ImageJ

plug-in MTrackJ (14). The emitted fluorescence was below the diffraction limit of the microscope, and therefore, each particle resembled a punctum of several graded bright pixels above background noise. The exact location was hard to resolve, but the ImageJ software allowed subpixel resolution by computing the centroid, or intensity-weighted mean position of the bright pixels that constitute the virion. Once the coordinates of each viral particle position across all frames in a movie were determined, the data were further analyzed using custom code written in Matlab.

SUPPLEMENTAL MATERIAL

Supplemental material for this article may be found at http://mbio.asm.org /lookup/suppl/doi:10.1128/mBio.00358-13/-/DCSupplemental.

Movie S1, AVI file, 11.2 MB.
Movie S2, AVI file, 5.6 MB.
Movie S3, AVI file, 10.7 MB.
Movie S4, AVI file, 9.1 MB.

ACKNOWLEDGMENTS

REFERENCES

1. **Pomeranz LE, Reynolds AE, Hengartner CJ.** 2005. Molecular biology of pseudorabies virus: impact on neurovirology and veterinary medicine. Microbiol. Mol. Biol. Rev. **69:**462–500.
2. **Ekstrand MI, Enquist LW, Pomeranz LE.** 2008. The alpha-herpesviruses: molecular pathfinders in nervous system circuits. Trends Mol. Med. **14:** 134–140.
3. **Field HJ, Hill TJ.** 1974. The pathogenesis of pseudorabies in mice following peripheral inoculation. J. Gen. Virol. **23:**145–157.
4. **McCracken RM, McFerran JB, Dow C.** 1973. The neural spread of pseudorabies virus in calves. J. Gen. Virol. **20:**17–28.
5. **Tannous R, Grose C.** 2011. Calculation of the anterograde velocity of varicella-zoster virions in a human sciatic nerve during shingles. J. Infect. Dis. **203:**324–326.
6. **Bearer EL, Breakefield XO, Schuback D, Reese TS, LaVail JH.** 2000. Retrograde axonal transport of herpes simplex virus: evidence for a single mechanism and a role for tegument. Proc. Natl. Acad. Sci. U. S. A. **97:** 8146–8150.
7. **Smith GA, Gross SP, Enquist LW.** 2001. Herpesviruses use bidirectional fast-axonal transport to spread in sensory neurons. Proc. Natl. Acad. Sci. U. S. A. **98:**3466–3470.
8. **Jansen AS, Ter Horst GJ, Mettenleiter TC, Loewy AD.** 1992. CNS cell groups projecting to the submandibular parasympathetic preganglionic neurons in the rat: a retrograde transneuronal viral cell body labeling study. Brain Res. **572:**253–260.
9. **Card JP, Enquist LW, Moore RY.** 1999. Neuroinvasiveness of pseudorabies virus injected intracerebrally is dependent on viral concentration and terminal field density. J. Comp. Neurol. **407:**438–452.
10. **Brittle EE, Reynolds AE, Enquist LW.** 2004. Two modes of pseudorabies virus neuroinvasion and lethality in mice. J. Virol. **78:**12951–12963.
11. **Klein RJ.** 1985. Initiation and maintenance of latent herpes simplex virus infections: the paradox of perpetual immobility and continuous movement. Rev. Infect. Dis. **7:**21–30.
12. **Roizman B, Sears AE.** 1987. An inquiry into the mechanisms of herpes simplex virus latency. Annu. Rev. Microbiol. **41:**543–571.
13. **del Rio T, Ch'ng TH, Flood EA, Gross SP, Enquist LW.** 2005. Heterogeneity of a fluorescent tegument component in single pseudorabies virus virions and enveloped axonal assemblies. J. Virol. **79:**3903–3919.
14. **Meijering E, Dzyubachyk O, Smal I.** 2012. Methods for cell and particle tracking. Methods Enzymol. **504:**183–200.
15. **Curanović D, Lyman MG, Bou-Abboud C, Card JP, Enquist LW.** 2009. Repair of the UL21 locus in pseudorabies virus Bartha enhances the kinetics of retrograde, transneuronal infection in vitro and in vivo. J. Virol. **83:**1173–1183.
16. **Taylor MP, Kramer T, Lyman MG, Kratchmarov R, Enquist LW.** 2012. Visualization of an alphaherpesvirus membrane protein that is essential for anterograde axonal spread of infection in neurons. mBio **3**(2):e00063-12. http://dx.doi.org/10.1128/mBio.00063-12.
17. **Purves D, Voyvodic JT, Magrassi L, Yawo H.** 1987. Nerve terminal remodeling visualized in living mice by repeated examination of the same neuron. Science **238:**1122–1126.
18. **Kramer T, Greco TM, Taylor MP, Ambrosini AE, Cristea IM, Enquist LW.** 2012. Kinesin-3 mediates axonal sorting and directional transport of alphaherpesvirus particles in neurons. Cell Host Microbe **12:**806–814.
19. **Antinone SE, Zaichick SV, Smith GA.** 2010. Resolving the assembly state of herpes simplex virus during axon transport by live-cell imaging. J. Virol. **84:**13019–13030.
20. **Mettenleiter TC.** 2000. Aujeszky's disease (pseudorabies) virus: the virus and molecular pathogenesis—state of the art, June 1999. Vet. Res. **31:** 99–115.
21. **Smith G.** 2012. Herpesvirus transport to the Nervous System and back again. Annu. Rev. Microbiol. **66:**153–176.
22. **Feierbach B, Piccinotti S, Bisher M, Denk W, Enquist LW.** 2006. Alpha-herpesvirus infection induces the formation of nuclear actin filaments. PLoS Pathog. **2:**e85. http://dx.doi.org/10.1371/journal.ppat .0020085.
23. **Granstedt AE, Kuhn B, Wang SS, Enquist LW.** 2010. Calcium imaging of neuronal circuits in vivo using a circuit-tracing pseudorabies virus. Cold Spring Harbor Protoc. 2010:pdb.prot5410. http://dx.doi.org/10 .1101/pdb.prot5410.